S. Ivansson. Two-dimensional anechoic diffraction grating coatings with noncircular scatterer cross-sections. Proceedings of the 36th Scandinavian Symposium on Physical Acoustics, Geilo February 2-6, 2013.

TWO-DIMENSIONAL ANECHOIC DIFFRACTION GRATING COATINGS WITH NONCIRCULAR SCATTERER CROSS-SECTIONS

Sven Ivansson[1]

[1]Swedish Defence Research Agency (FOI), SE-16490 Stockholm, Sweden, email: sven.ivansson@foi.se

Abstract

A thin rubber coating with cavities in a periodic lattice can redistribute sound energy, normally incident on a steel plate in water, in the lateral direction. The scattered energy can be absorbed by the rubber material and the reflection amplitude in the water can be reduced significantly. Coatings with different geometric cavity types are here compared: spheres, (super)ellipsoids, cylinders with circular cross-sections, and cylinders with (super)elliptic cross-sections. In the latter cases, the cylinder axes are parallel to the coating. Spheres and (super)ellipsoids appear in a doubly periodic lattice, while the cylinders appear in a lattice with a single period. Each coating type is optimized by differential evolution, varying a number of material and geometrical parameters to minimize the maximum reflectance within a certain frequency band. The layer multiple-scattering method is used as forward model. To achieve good low-frequency broad-band reflectance reduction with a thin coating, it is advantageous to extend the cavities in the lateral directions and to mix cavities of different sizes. Very good results are obtained for cylindrical cavities with superelliptic cross-sections.

1 Introduction

Phononic crystals (PC) have mainly been applied to sound shielding, i.e., reduction of sound transmission, but reduction of sound reflections has also been considered. One particular application of the latter type concerns underwater anechoic coatings of Alberich type, i.e., rubber coatings with a periodic lattice of cavities or other scatterers. A coating should be thin and provide significant reflection reduction over a broad frequency band. The design problem can be formulated numerically as a nonlinear optimization problem. Hence, global optimization techniques from inverse theory can be applied, such as differential evolution (DE) [1].

For cavities in a doubly periodic lattice, results in [2] show that extension of spheres in the lateral direction, to form oblate superellipsoids, is useful to obtain good reflectance reduction at low frequencies with a thin coating. Infinite extension of a sphere in one lateral direction leads to a cylinder with circular cross-section. Such cavities are considered in [3]. Again, the extension is seen to promote reflection reduction efficiency at low frequencies. In the mentioned papers, DE is used for coating optimization with the layer multiple scattering (LMS) method as forward model. Cavities of one and two sizes are considered.

In the present paper, the cylinders are extended in the orthogonal lateral direction to produce oblate superelliptic cross-sections. Transition matrices (T-matrices) of such cavities, needed for the LMS method, are computed by adapting a null-field approach for smooth rotationally symmetric 3-D bodies by Boström [4] to the 2-D case. Coatings with different geometric cavity types are compared. Some design results from [2], for coatings with sphere and superellipsoid cavities, are first recapitulated in Secs. 2 and 3, respectively. Corresponding design examples with cylindrical cavities are subsequently studied in Sec. 4, for cylinders with spherical cross-sections, and in Sec. 5, for cylinders with superelliptic cross-sections. Scattering and absorption cross-sections are computed for isolated cavities of the different shapes to better understand the coating design results.

2 Coatings with sphere cavities

Fig. 1 shows a steel plate that is coated by a rubber layer with spherical cavities. The cavities appear in a doubly periodic lattice with period d. All cavities in panel (a) are of the same size, case (a), whereas there are two cavity sizes in panel (b), case (b). A Cartesian xyz coordinate system is introduced, and a monofrequency plane sound wave is normally incident from the water half-space on top. All the time, all cavities are placed at the bottom of the coating, in direct contact with the steel plate.

Parameters for steel are fixed at 5850 and 3230 m/s for the compressional- and shear-wave velocities, respectively, and 7700 kg/m^3 for the density. The sound velocity of water is 1480 m/s. Only the rubber is anelastic, with a shear-wave absorption of 25 dB/wavelength. The compressional-wave absorption for the rubber is either set to the least value consistent with the physical constraint for the bulk modulus (case $P_{absorp}min$) or to 10 dB/wavelength (case $P_{absorp}10$).

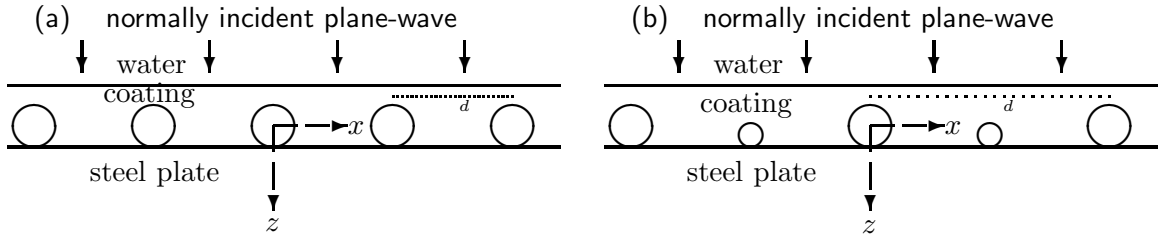

Figure 1: A steel plate is covered with an Alberich rubber coating with sphere cavities in a square lattice with period d. Case (a) in the left panel involves one cavity type, whereas case (b) in the right panel involves two cavity types. In each case, Cartesian xyz coordinates are shown, with the y axis going out of the paper plane. The cavity lattice has period d in x as well as y, and the lattice for the small spheres in case (b) is displaced $d/2$ not only in the x direction but also in the y direction.

The objective function, for DE minimization in the coating design examples to follow, is specified as the maximum reflectance in the frequency band 8-22 kHz. Reflectance is here time- (and space-) averaged reflected energy flux relative to the time-averaged energy flux of the normally incident monofrequency plane wave in the water.

Eight design parameters, denoted p_1,p_2,...,p_8, are varied within the following search space for the DE minimization: lattice period [$p_1 = d$, with least distance between cavities in 2-80 mm], coating thickness [$p_2 = H$, 0.5-12 mm], fraction of coating thick-

ness between water and closest cavity surface [p_3, 0.2-0.94 and 0.2-0.8 for cases (a) and (b), respectively], cavity excentricity parameter [$p_4 = a/b$, to become relevant in Secs. 3 and 5], quotient between the length-scale sizes of the smallest and the largest cavities [$p_5 = q$, 0.15-1.0, relevant only for case (b)], rubber compressional-wave velocity [$p_6 = \alpha$, 1400-1600 m/s]. rubber shear-wave velocity [$p_7 = \beta$, 60-400 m/s], and rubber density [p_6, 900-1300 kg/m^3].

The design results are shown in Fig. 2, for the four cases $P_{absorp}min$ (a), $P_{absorp}min$ (b), and $P_{absorp}10$ (a), $P_{absorp}10$ (b). Corresponding optimal parameter values are provided in Table I.

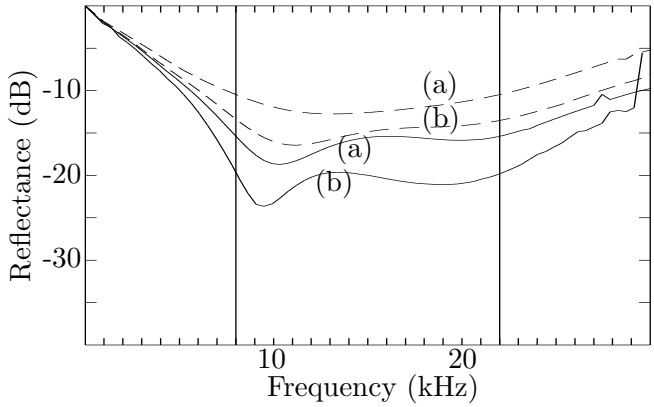

Figure 2: Reflectancies in decibel as functions of frequency obtained by differential evolution [1] optimization for coatings with sphere cavities. Case (a) involves one cavity type (left panel of Fig. 1), whereas case (b) involves two cavity types (right panel of Fig. 1). Rubber materials with minimal and 10 dB/wavelength compressional-wave absorption are prescribed for the dashed-line and solid-line results, respectively. The coatings are specified in Table I. It is the largest reflectance within the band 8-22 kHz, marked with vertical lines, that is minimized.

Table I. Specification of optimized coatings for the curves of Fig. 2.

	$P_{absorp}min$ (a)	$P_{absorp}min$ (b)	$P_{absorp}10$ (a)	$P_{absorp}10$ (b)
optimum (dB)	-10.4	-13.7	-14.8	-20.0
$p_1 = d$ (mm)	30.1	35.0	37.2	42.6
$p_2 = H$ (mm)	12.0	12.0	12.0	12.0
p_3	0.20	0.20	0.20	0.20
$p_4 = a/b$	1	1	1	1
$p_5 = q$	-	0.42	-	0.45
$p_6 = \alpha$ (m/s)	1400.0	1400.0	1401.0	1401.0
$p_7 = \beta$ (m/s)	190.3	159.1	160.4	139.9
$p_8 = \rho$ (kg/m^3)	1143.5	1171.7	1179.7	1160.6

3 Coatings with superellipsoid cavities

Following [2], the spherical cavities from Sec. 2 are now replaced by superellipsoidal ones. In a local centered coordinate system, with horizontal coordinates x,y and a

depth coordinate z, the equation of the cavity surface is

$$\left(\frac{|z|}{a}\right)^p + \left(\frac{r}{b}\right)^p = 1 \ , \tag{3.1}$$

where $r = |(x, y)|$. In its local coordinate system, each cavity is apparently symmetric with respect to rotation around the z axis. Fig. 3 shows a coated steel plate with the spheres from Fig. 1 replaced by superellipsoids.

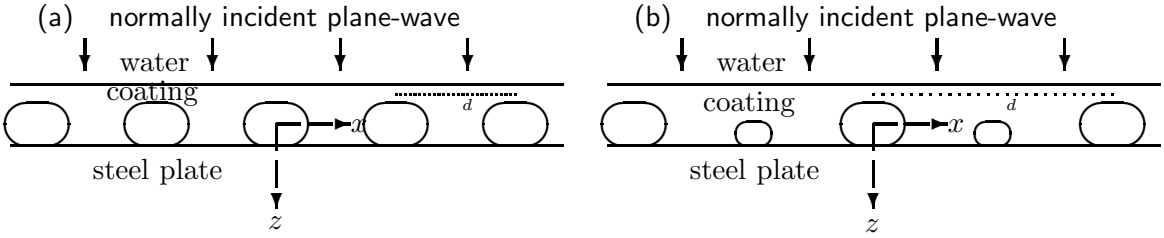

Figure 3: A coated steel plate as in Fig. 1 but with superellipsoid cavities.

Coating design results, corresponding to those in Fig. 2 and Table I, are shown in Fig. 4 and Table II. The shape exponent p from Eq. (3.1) is fixed at four for all cavities. The previously irrelevant design parameter p_4 for cavity excentricity is now active with search interval according to [$p_4 = a/b$ from Eq. (3.1), 0.4-1.0]. For case (b) with two types of cavities present, they differ in size but not in shape. Specifically, the quotient a/b, with a and b from Eq. (3.1), is the same for both types. The classical Meyer *et al.* [5] monopole scattering resonance, for a spherical cavity in an elastic solid with a reasonably small shear-wave velocity, is crucial for the echo reduction effect of an Alberich coating. It appears when the circumference equals two shear-wave wavelengths in the solid. Examples in [2] illustrate how this resonance is changed when the shape of the cavity is changed from spherical to (super)ellipsoidal.

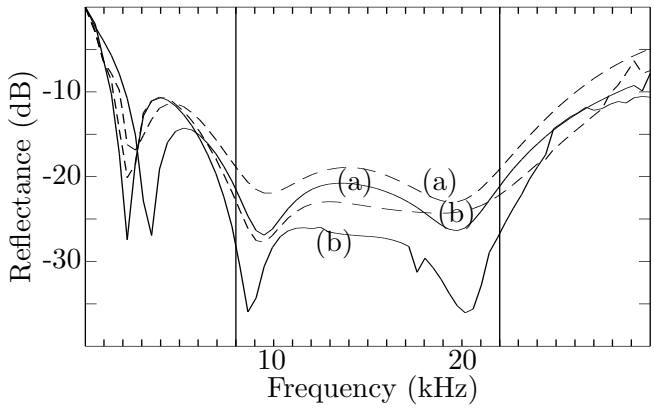

Figure 4: Reflectancies in decibel for optimized coatings as in Fig. 2 but for superellipsoid cavities. Case (a) involves one cavity type (left panel of Fig. 3), whereas case (b) involves two cavity types (right panel of Fig. 3). Rubber materials with minimal and 10 dB/wavelength compressional-wave absorption are prescribed for the dashed-line and solid-line results, respectively. The coatings are specified in Table II.

Table II. Specification of optimized coatings for the curves of Fig. 4.

	$P_{absorp}min$ (a)	$P_{absorp}min$ (b)	$P_{absorp}10$ (a)	$P_{absorp}10$ (b)
optimum (dB)	-18.9	-22.2	-20.8	-26.0
$p_1 = d$ (mm)	46.8	53.4	49.9	60.5
$p_2 = H$ (mm)	11.9	12.0	12.0	12.0
p_3	0.20	0.20	0.29	0.22
$p_4 = a/b$	0.41	0.40	0.40	0.41
$p_5 = q$	-	0.40	-	0.44
$p_6 = \alpha$ (m/s)	1427.1	1400.7	1400.9	1413.8
$p_7 = \beta$ (m/s)	332.3	280.3	265.2	239.9
$p_8 = \rho$ (kg/m^3)	1214.3	1257.2	1225.0	1225.8

Consider a rubber material with $\beta/\alpha = 0.2$, where α and β are the compressional- and shear-wave velocities, respectively. Three different kinds of cavities are chosen, all with the same height $2a$: (a) a sphere with radius a, (b) an ellipsoid with parameters $b = 2a$, p=2 from Eq. (3.1), and (c) a superellipsoid with $b = 2a$, p=4. They are illustrated in the left panel of Fig. 5. The solid-line scattering cross-section curves (a), (b), and (c) in the right panel of Fig. 5, computed with the T-matrix method, show resonances at fa, in kHz mm, about 96 for the sphere, 60 for the ellipsoid, and 56 for the superellipsoid. Here, f denotes the frequency. A plane compressional wave is incident from above, propagating downwards in the direction of increasing z, cf. Eq. (3.1). The scattering cross-sections in the figure are all given relative to the area $4a^2\pi$, which agrees with the geometrical cross-sectional area for the ellipsoid and superellipsoid cavities.

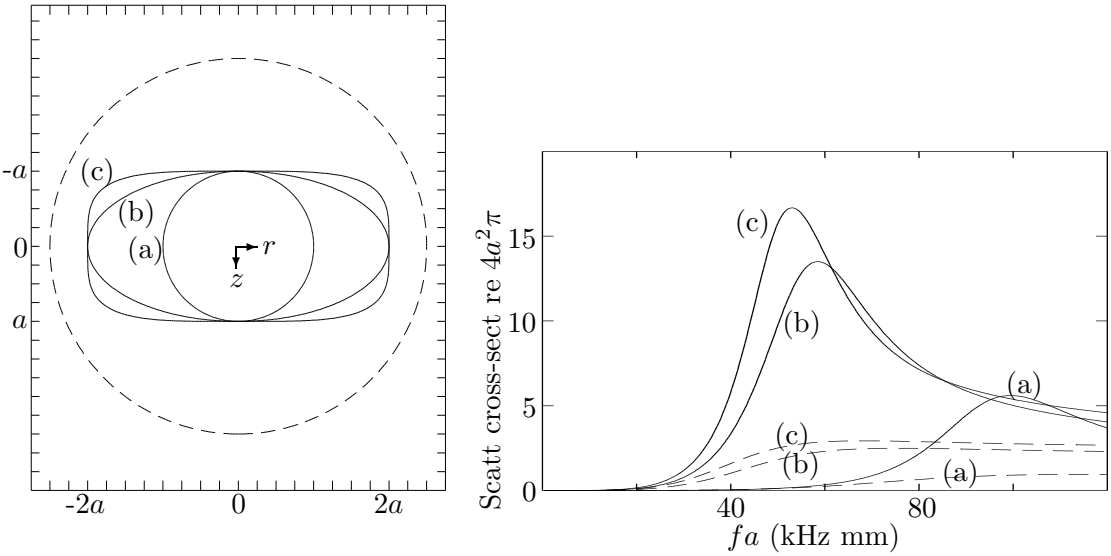

Figure 5: *Left panel:* Shapes of three cavities (a) a sphere with radius a, (b) an ellipsoid with parameters a, $b = 2a$, p=2, as defined in Eq. (3.1), and (c) a superellipsoid with parameters a, $b = 2a$, p=4. The dashed curve shows an enclosing sphere with radius $5a/2$. *Right panel:* Total scattering cross-sections for the three cavity types (a), (b), and (c), in rubber with $\beta/\alpha = 0.2$. They are given in units of the geometrical cross-sectional area $4a^2\pi$ for the ellipsoid and superellipsoid cavities. A compressional plane wave is incident from above. There is no absorption for the solid-line curves, whereas the dashed-line ones concern cases with a shear-wave absorption of 20 dB per wavelength.

No absorption is involved for the solid-line curves in the right panel of Fig. 5. Including a rubber shear-wave absorption of 20 dB per wavelength, the resonance effect is not clearly seen at long ranges any more, and the dashed-line scattering cross-section curves are obtained.

Absorption cross-sections are shown in Fig. 6, for the three chosen cavity types, for a rubber shear-wave absorption of 20 dB per wavelength. They were computed using the T-matrix method in connection with formulas such as Eq. (24) of Ref. [6]. As before, a plane compressional wave is incident from above, and the cross-sections are given in units of $4a^2\pi$. Interaction with the incident field is included, in contrast to the scattering cross-sections of Fig. 5, which only involve the scattered field.

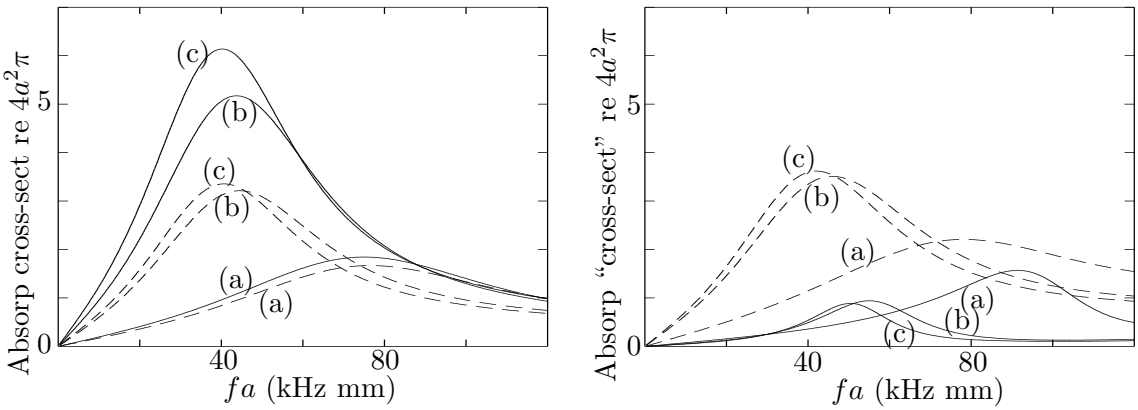

Figure 6: Absorption cross-sections for the three cavity types (a), (b), and (c) from the left panel of Fig. 5, in rubber with $\beta/\alpha = 0.2$. *Left panel:* The total absorption cross-sections are shown by the solid-line curves, whereas the dashed-line ones only concern the losses suffered within a surrounding sphere with radius $5a/2$. *Right panel:* Compressional-wave absorption of 10 dB/wavelength is included here. The absorbed power within a surrounding sphere with radius $5a/2$ is divided by a reference intensity, taken as the incident wave intensity at the horizontal center level $z = 0$. There is only compressional-wave absorption for the solid-line curves, whereas a rubber shear-wave absorption of 20 dB/wavelength is included for the dashed-line ones.

In comparison to the resonance frequencies seen in the solid-line curves in the right panel of Fig. 5, the frequencies of maximum absorbance from Fig. 6 are shifted slightly downwards. The peak frequency is still decreased as the volume of the cavity is increased.

The dashed-line curves in the left panel of Fig. 6 show how much of the loss that is suffered within the enclosing sphere of radius $5a/2$ that is depicted in the left panel of Fig. 5. As expected from Ref. [6], most of the lost energy is absorbed close to the cavity.

The resonance frequency of an individual cavity can be lowered by increasing its volume or by decreasing the rubber shear-wave velocity. Hence, for a fixed coating layer thickness and a fixed rubber shear-wave velocity, oblate ellipsoidal or superellipsoidal shapes seem appropriate to get a thin coating for low frequencies. For the example with cavity height limited to $2a$ and $\beta/\alpha = 0.2$, Figs. 5 and 6 show that a coating with spherical cavities would have much higher single-cavity resonance frequencies.

The right panel of Fig. 6 shows absorption cross-section results when rubber compressional-wave absorption of 10 dB/wavelength is included. The spherical, ellipsoidal, and superellipsoidal cavities from the left panel of Fig. 5 are still used. With losses

already in the incident compressional wave, the incident wave intensity now decreases with increasing z and the definition of an absorption cross-section becomes less obvious. The "close-range cross-sections" in the right panel of Fig. 6 concern the absorbed power within the $5a/2$ radius sphere surrounding a cavity, divided by the incident wave intensity at the horizontal center level $z = 0$. No shear-wave absorption is introduced for the solid-line curves, whereas the shear-wave absorption is 20 dB/wavelength for the dashed-line ones.

4 Coatings with circle-cylinder cavities

A sphere can be transformed to a cylinder, with circular cross-section, by extension in one lateral direction. Fig. 7, taken from [3], shows how the resonance frequencies, expressed as $k_s a = \omega a/\beta$ where $\omega = 2\pi f$ is the angular frequency, vary with β/α for a sphere and a circle-cylinder. A monofrequency radially symmetric compressional wave is normally incident on the cavity. As β/α decreases, the resonance frequencies for the fundamental T-matrix element approach the ones for the cavity surface displacement amplitude from above, in the sphere as well as cylinder cases.

An important observation is that the resonance frequencies for the cylinder are much smaller than those for a sphere of the same radius. For the β/α values considered in Fig. 7, the displacement amplitude resonance frequencies for the cylinder are less than half of those for the sphere. As β/α decreases to zero, the resonance frequencies for the cylinder decrease towards zero as well.

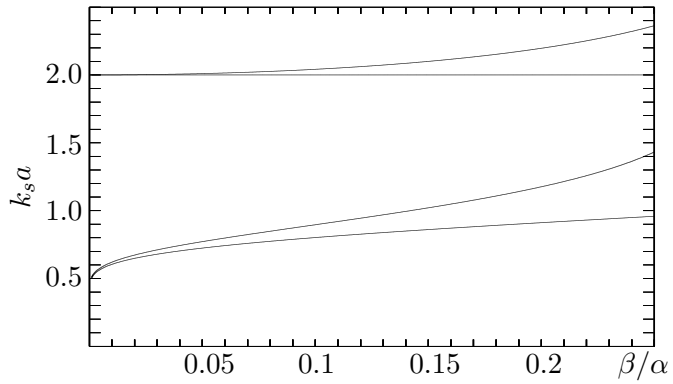

Figure 7: Resonance scattering by a spherical (the two upper curves) or cylindrical (the two lower curves) cavity in a homogeneous solid medium. In each case, the uppermost and lowermost curves indicate the (lowest) resonances for the fundamental T-matrix element and the cavity surface displacement, respectively.

It is thus of interest to design optimal coatings as in Secs. 2 and 3 but for circle-cylinder cavities as depicted in Fig. 8. The computations can be performed in 2-D, since the wave fields are now independent of the y coordinate. The LMS method for computation of scattering by a phononic crystal slab is described in a unified way for 3-D and 2-D cases in [3, Sec. III]. Handling of different types of scatterers at the same interface is also treated in [7, Sec. 3], including computation of transition matrices for vertically displaced scatterers.

The design results for coatings with circle-cylinder cavities are shown in Fig. 9 and

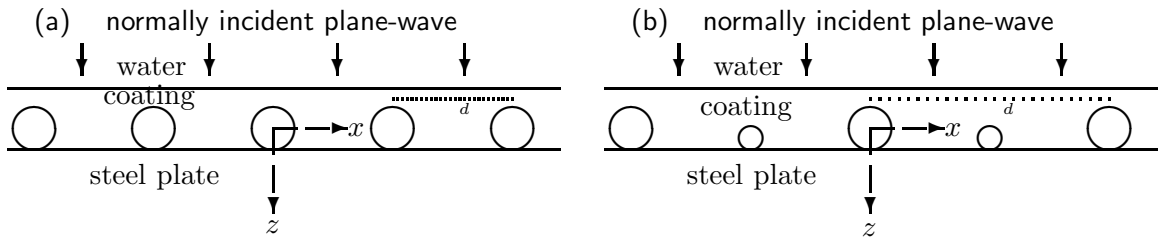

Figure 8: A steel plate is covered with an Alberich rubber coating with circle-cylinder cavities in a lattice with period d. Case (a) in the left panel involves one cavity type, whereas case (b) in the right panel involves two cavity types. In each case, Cartesian xyz coordinates are shown, with the y axis going out of the paper plane. The cavity lattice has a single period d, in x.

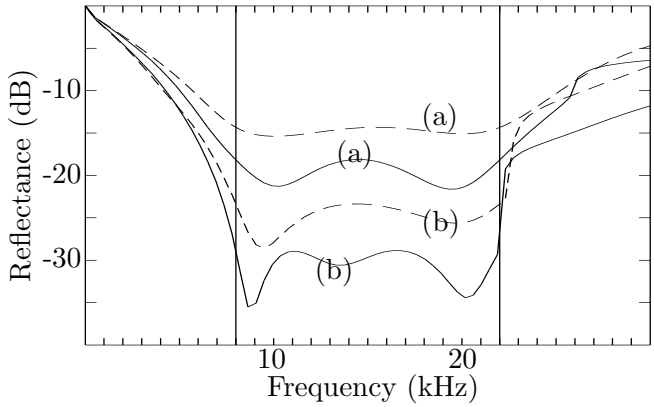

Figure 9: Reflectancies in decibel for optimized coatings as in Figs. 2 and 4 but for circle-cylinder cavities. Case (a) involves one cavity type (left panel of Fig. 8), whereas case (b) involves two cavity types (right panel of Fig. 8). Rubber materials with minimal and 10 dB/wavelength compressional-wave absorption are prescribed for the dashed-line and solid-line results, respectively. The coatings are specified in Table III. It is the largest reflectance within the band 8-22 kHz, marked with vertical lines, that is minimized.

Table III. Specification of optimized coatings for the curves of Fig. 9.

	$P_{absorp}min$ (a)	$P_{absorp}min$ (b)	$P_{absorp}10$ (a)	$P_{absorp}10$ (b)
optimum (dB)	-14.3	-23.4	-18.2	-28.9
$p_1 = d$ (mm)	45.9	65.5	57.1	67.3
$p_2 = H$ (mm)	12.0	10.8	12.0	12.0
p_3	0.20	0.43	0.20	0.70
$p_4 = a/b$	1	1	1	1
$p_5 = q$	-	0.30	-	0.32
$p_6 = \alpha$ (m/s)	1412.9	1400.0	1464.5	1400.0
$p_7 = \beta$ (m/s)	368.7	176.5	352.0	110.6
$p_8 = \rho$ (kg/m^3)	1300.0	1034.8	1300.0	1002.8

Table III. Compared to the results for spheres in Sec. 2, significant improvements can be noted. Particularly the case (b) results are competitive in comparison to Fig. 4 in Sec. 3 as well. It is worth observing that the optimal p_3 parameter values in Table III, for outer coating thickness fraction, are as large as 0.43 and 0.70 for the two (b) cases, respectively. These values are much larger than the lower search interval limit 0.20, indicating that small cylinder radii provide resonance frequencies that are low enough,

and that very good performance could presumably be obtained with significantly thinner coatings.

5 Coatings with superellipse-cylinder cavities

The coatings with sphere cavities in Fig. 1 of Sec. 2 were extended in Sec. 3 to coatings with superellipsoid cavities according to Fig. 3. It is now natural to extend the coatings with circle-cylinder cavities in Fig. 8 of Sec. 4 to coatings with superellipse-cylinder cavities as in Fig. 10.

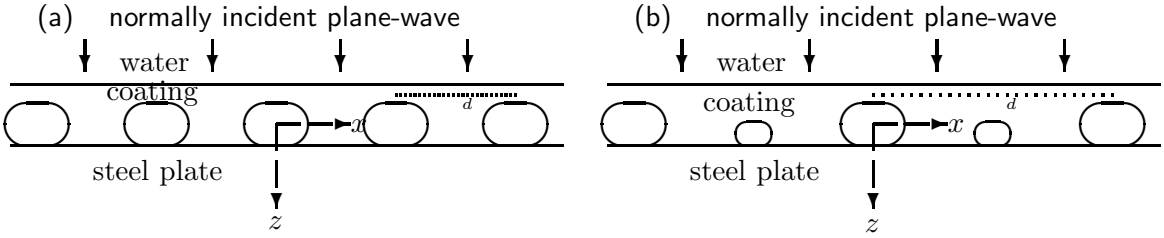

Figure 10: A coated steel plate as in Fig. 8 but with superellipse-cylinder cavities.

The required extension of the LMS computational method, to cylindrical scatterers with noncircular cross-sections, is outlined in [7, Sec. 3.C]. In general, the transition matrix T must now be computed numerically, with the null field approach, for example. As described in [8], [9], general representation formulas are used to express the expansion coefficients of the incident and the scattered fields, respectively, in terms of integrals of displacements and tractions over the scatterer surface. The surface fields are expanded in some suitable basis of vector wave functions, and the desired T-matrix is obtained by matrix inversion followed by matrix multiplication. In a suitable cylindrical vector solution basis, the transition matrix T is symmetric, which can be used to check the accuracy.

Coating design results for the superellipse-cylinder cavities, corresponding to the results in Fig. 9 and Table III, are shown in Fig. 11 and Table IV. In a local centered coordinate system, with horizontal coordinates x,y and a depth coordinate z, the equation of the superelliptical cavity surface is

$$\left(\frac{|z|}{a}\right)^p + \left(\frac{|x|}{b}\right)^p = 1 \ . \tag{5.1}$$

The shape exponent p is fixed at four for all cavities. As in Sec. 3, the design parameter p_4 for cavity excentricity is now active with search interval according to [$p_4 = a/b$ from Eq. (5.1), 0.4-1.0]. For case (b) with two types of cavities present, they differ in size but not in shape. Specifically, the quotient a/b, with a and b from Eq. (5.1), is the same for both types.

The optimal p_3 parameter values in Table IV, for outer coating thickness fraction, are large in all cases, with values between 0.55 and 0.75. It was noted already in connection with Table III that such large values, much larger than the lower search interval limit 0.20, indicate that very good performance could presumably be obtained

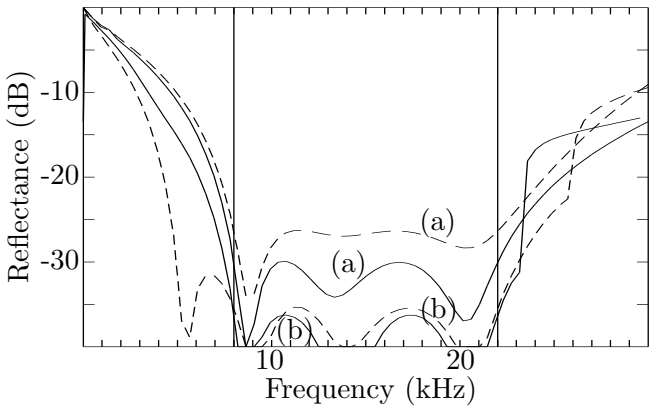

Figure 11: Reflectancies in decibel for optimized coatings as in Fig. 9 but for superellipse-cylinder cavities. Case (a) involves one cavity type (left panel of Fig. 10), whereas case (b) involves two cavity types (right panel of Fig. 10). Rubber materials with minimal and 10 dB/wavelength compressional-wave absorption are prescribed for the dashed-line and solid-line results, respectively. The coatings are specified in Table IV.

with significantly thinner coatings.

Table IV. Specification of optimized coatings for the curves of Fig. 11.

	$P_{absorp}min$ (a)	$P_{absorp}min$ (b)	$P_{absorp}10$ (a)	$P_{absorp}10$ (b)
optimum (dB)	-26.4	-35.5	-30.0	-36.4
$p_1 = d$ (mm)	43.4	57.0	42.0	64.4
$p_2 = H$ (mm)	11.6	8.0	8.6	10.3
p_3	0.55	0.56	0.55	0.75
$p_4 = a/b$	0.40	0.40	0.40	0.40
$p_5 = q$	-	0.33	-	0.33
$p_6 = \alpha$ (m/s)	1400.0	1400.0	1400.0	1481.8
$p_7 = \beta$ (m/s)	400.0	208.3	334.6	154.4
$p_8 = \rho$ (kg/m^3)	1185.4	912.7	1059.7	900.0

As in Sec. 3, it is useful to study scattering and absorption cross-sections for an isolated cavity in order to understand the improved echo reduction obtained by extending the cavities laterally. The T-matrix method can be used to compute the cross-sections, in connection with formulas such as [7, (61)-(62)]. Fig. 12 and Fig. 13 show results corresponding to those in Fig. 5 and Fig. 6, respectively. The rubber shear- and compressional-wave velocities β and α still fulfil $\beta/\alpha = 0.2$ in these examples. As before, a plane compressional wave is incident from above, but the cross-sections are now given in units of $4a$, which is the geometrical cross-sectional length for the ellipse and superellipse cavities.

Figs. 12 and 13 show that fa at cavity resonance is lowered when the cylinder cross-section is extended in the lateral direction, orthogonal to the direction of the incident plane compressional wave. Moreover, as seen by a comparison to Figs. 5 and 6, 2-D cylindrical cavities provide significantly lower resonance fa values than corresponding 3-D cavities that are rotationally invariant in the lateral directions.

It is informative to consider the cavity half-heights a for the optimal coatings according to Table IV. For the $P_{absorp}10$ (a) case, for example, one has $a = 1.93$ mm.

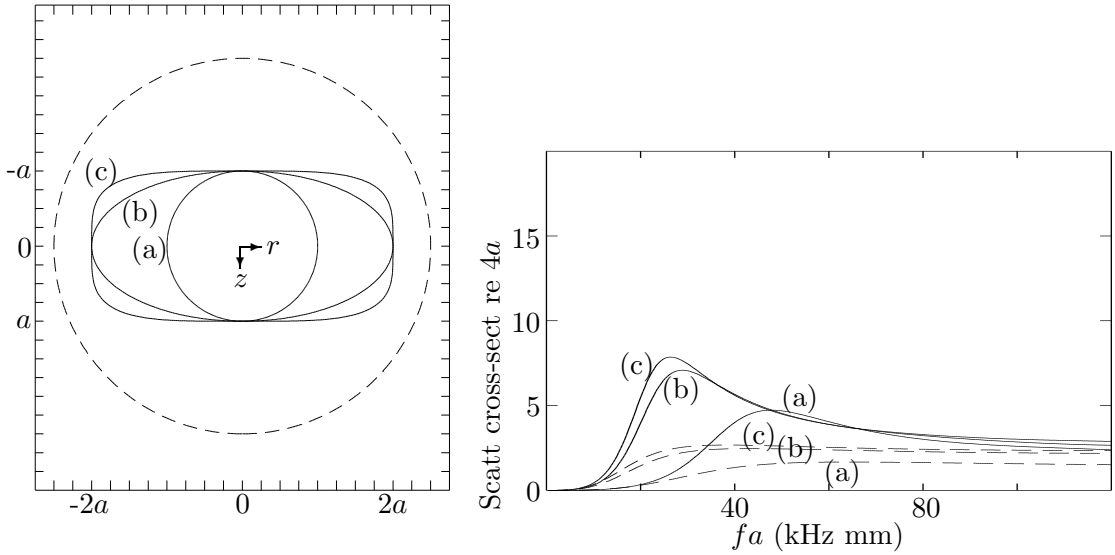

Figure 12: *Left panel:* Shapes of three cavities (a) a circle-cylinder with radius a, (b) an ellipse-cylinder with parameters a, $b = 2a$, p=2, as defined in Eq. (5.1), and (c) a superellipse-cylinder with parameters a, $b = 2a$, p=4. The dashed curve shows an enclosing cylinder with circular cross-section and radius $5a/2$. *Right panel:* Total scattering cross-sections for the three cavity types (a), (b), and (c), in rubber with $\beta/\alpha = 0.2$. They are given in units of the geometrical cross-sectional length $4a$ for the cavities with elliptic and superelliptic cavities. A compressional plane wave is incident from above. There is no absorption for the solid-line curves, whereas the dashed-line ones concern cases with a shear-wave absorption of 20 dB per wavelength.

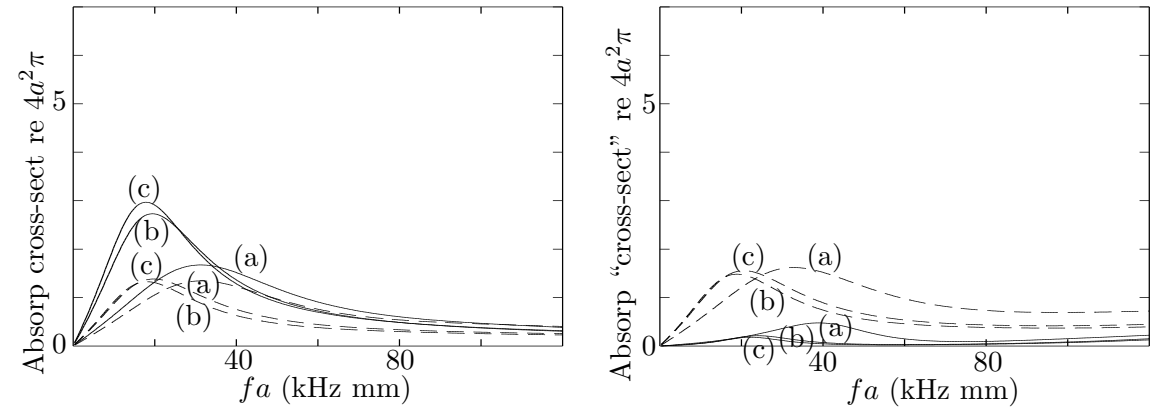

Figure 13: Absorption cross-sections for the three cavity types (a), (b), and (c) from the left panel of Fig. 12, in rubber with $\beta/\alpha = 0.2$. *Left panel:* The total absorption cross-sections are shown by the solid-line curves, whereas the dashed-line ones only concern the losses suffered within a surrounding sphere with radius $5a/2$. *Right panel:* Compressional-wave absorption of 10 dB/wavelength is included here. The absorbed power within a surrounding sphere with radius $5a/2$ is divided by a reference intensity, taken as the incident wave intensity at the horizontal center level $z = 0$. There is only compressional-wave absorption for the solid-line curves, whereas a rubber shear-wave absorption of 20 dB/wavelength is included for the dashed-line ones.

With 8 kHz $< f <$ 22 kHz, this corresponds to 15.4 kHz mm $< fa <$ 42.5 kHz mm. Comparison can be made to the dashed-line (c) curve in the right panel of Fig. 13, although $\beta/\alpha = 334.6/1400 = 0.24$ is slightly different from 0.2 and the shear-wave absorption 25 dB/wavelength is slightly different from 20 dB/wavelength. As expected, a large single-cavity absorption effect appears for fa in the interval (15.4,42.5) kHz mm.

6 Conclusions

Significant echo reduction can be achieved by rubber coatings with cavities arranged in a periodic fashion. Incident sound energy is scattered by the cavities, which promotes absorption in the rubber material of the coating. The effect appears for frequencies in the vicinity of the cavity resonance frequencies, and it is useful to mix cavities of at least two sizes to obtain broad-band echo reduction.

Cavities of different shapes are compared in the present paper, concerning their echo reduction capability. Thin coatings with effect at low frequencies are desired, indicating a need of low fa values at resonance for the coating cavities. Here, f is the frequency and a is half the cavity height. It is seen that the fa resonance values can be lowered by extending the cavities in the lateral directions, parallel to the coating. Cavities of 3-D type according to Eq. (3.1), with rotational invariance in the lateral directions, are compared to 2-D cylinder cavities according to Eq. (5.1), with infinite extension in one of the lateral directions. In these equations, b denotes lateral cavity half-axis length. For the same excentricity (same a/b value), the 2-D cylinder cavity gives a much lower value of fa at resonance than does the 3-D cavity. A much larger excentricity would be needed for the 3-D cavity, to compensate the infinite extension of the 2-D cylinder in one of the lateral directions, and the lattice period d imposes constraints on the excentricity.

References

[1] Price, K., Storn, R., and Lampinen, J., 2005. *Differential Evolution - A Practical Approach to Global Optimization* (Springer, New York).

[2] Ivansson, S., 2008. Numerical design of Alberich anechoic coatings with superellipsoidal cavities of mixed sizes. J. Acoust. Soc. Am. **124**, 1974-1984; **131**, 3180(E) (2012).

[3] Ivansson, S., 2012. Anechoic coatings obtained from two- and three-dimensional monopole resonance diffraction gratings. J. Acoust. Soc. Am. **131**, 2622-2637.

[4] Boström, A., 1980. Scattering by a smooth elastic obstacle. J. Acoust. Soc. Am. **67**, 1904-1913.

[5] Meyer, E., Brendel, K., and Tamm, K., 1958. Pulsation oscillations of cavities in rubber. J. Acoust. Soc. Am. **30**, 1116-1120.

[6] Ivansson, S., 2006. Sound absorption by viscoelastic coatings with periodically distributed cavities. J. Acoust. Soc. Am. **119**, 3558-3567.

[7] Ivansson, S., 2008. Extended layer multiple-scattering and global optimization techniques for 2D phononic crystal insulator design. In *Photonic research developments*, edited by Nilsson, V., (Nova), pp. 225-245. The quantities Δ in Eqs. (10) and (26) additionally depend on sign(z). Furthermore, the transition matrix T is in general symmetric only after a simple change of cylindrical vector solution basis.

[8] Varadan, V.V., 1979. Scattering matrix for elastic waves II Application to elliptic cylinders. J. Acoust. Soc. Am. **65**, 896-905.

[9] Radlinski, R.P., and Simon, M.M., 1993. Acoustic and elastic wave scattering from elliptic-cylindrical shells. J. Acoust. Soc. Am. **93**, 2443-2453.